JM RAPIDS

Non-monotonic effect of compaction on longitudinal dispersion coefficient of porous media

Yang Liu[1], Wenbo Gong[1], Han Xiao[1] and Moran Wang[1],†

[1]Department of Engineering Mechanics, Tsinghua University, Beijing 100084, China

Utilizing the discrete element method and the pore network model, we numerically investigate the impact of compaction on the longitudinal dispersion coefficient of porous media. Notably, the dispersion coefficient exhibits a non-monotonic dependence on the degree of compaction, which is distinguished by the presence of three distinct regimes in the variation of dispersion coefficient. The non-monotonic variation of dispersion coefficient is attributed to the disparate effect of compaction on dispersion mechanisms. Specifically, the porous medium tightens with an increasing pressure load, reducing the effect of molecular diffusion that primarily governs at small Péclet numbers. On the other hand, heightened pressure loads enhance the heterogeneity of pore structures, resulting in increased disorder and a higher proportion of stagnant zones within porous media flow. These enhancements further strengthen mechanical dispersion and hold-up dispersion, respectively, both acting at higher Péclet numbers. It is crucial to highlight that hold-up dispersion is induced by the low-velocity regions in porous media flow, which differ fundamentally from zero-velocity regions (such as dead-ends or the interior of permeable grains) as described by the classical theory of dispersion. The competition between weakened molecular diffusion and enhanced hold-up dispersion and mechanical dispersion, together with the shift in the dominance of dispersion mechanisms across various Péclet numbers, results in multiple regimes in the variation of dispersion coefficients. Our study provides unique insights into structural design and modulation of the dispersion coefficient of porous materials.

Key words: porous media, dispersion

† Email address for correspondence: moralwang@jhu.edu

988 R2-1

1. Introduction

Solute transport through porous media is prevalent in numerous industrial applications, such as fixed-bed reactors (Jurtz, Kraume & Wehinger 2019), carbon dioxide geological sequestration (Bolster 2014; Amooie, Soltanian & Moortgat 2018), etc., thus making it a classic topic of research (Saffman 1959; Koch & Brady 1985; Sahimi *et al.* 1986; Bijeljic, Muggeridge & Blunt 2004; Borgne *et al.* 2010; Puyguiraud, Gouze & Dentz 2021; Bordoloi *et al.* 2022; Dentz *et al.* 2022). Porous media are regularly subjected to in-situ stresses originating from various sources such as high-pressure injection (Morris *et al.* 2011; Ranjith & Perera 2011; Ringrose *et al.* 2013), thermal stresses within the geothermal system (Chen, Jin & Wang 2018) and geologic stresses at different depths in the formation (Kang *et al.* 2019). These stressors bring about alterations in the pore structure, for instance, ground uplift by carbon dioxide injection in the In Salah formation (Morris *et al.* 2011; Ringrose *et al.* 2013), thereby potentially exerting a significant impact on the dynamics of flow and mass transfer. The dispersion coefficient is one of the key parameters that governs solute transport through porous media, reflecting the ability to attenuate concentration gradients (Dentz, Hidalgo & Lester 2023). The impact of compaction on the dispersion coefficient of the porous medium has attracted extensive research interest. Numerous studies have focused on the areas of subsurface disposal of radioactive waste and compaction of soils. The scenarios covered in these studies are mostly at small Péclet number *Pe*, indicating that the dispersion coefficient of the porous medium tends to decrease with the degree of compaction (Hamamoto *et al.* 2009; Kuncoro *et al.* 2014). Nevertheless, contrasting trends are observed in other investigations related to chromatographic separation, occurring at larger *Pe*. These studies demonstrate an entirely opposite trend, whereby an increase in the degree of compaction leads to a noticeable rise in the dispersion coefficient of the porous medium (Charlaix, Hulin & Plona 1987; Huh, Charlaix & Plona 1988; Östergren & Trägårdh 2000). In addition, multiple studies focused on the dispersion coefficient of rocks present consistent results: the dispersion coefficient shows a completely opposite dependence on the degree of consolidation across distinct ranges of *Pe* (Bijeljic, Mostaghimi & Blunt 2011; Goldobin 2011; Boon, Bijeljic & Krevor 2017).

Despite the widespread acknowledgment of the non-trivial dependence between the dispersion coefficient and the degree of compaction, research progress on the understanding and mechanism explanation of this phenomenon is still very limited. Numerical simulation is a powerful tool for elucidating the microscopic mechanisms of macroscopic phenomena, yet there are challenges in trading off the accuracy and efficiency of numerical methods. The majority of numerical investigations concerning the impact of compaction on solute transport through porous media have adopted continuum-based methods (Smith 2000; Peters & Smith 2002; Qiu, Chen & Tong 2022). While these methods demonstrate efficiency, they fail to resolve the changes in the microstructure, a determinant that profoundly influences flow and transport. On the other hand, a precise representation of pore structure evolution in response to pressure loads, along with accurate modelling of solute transport across a wide range of *Pe*, encounters computational constraints. The discrete element method (DEM) is a particle-based approach designed to simulate the dynamic behaviour of granular materials subjected to external forces (Potyondy & Cundall 2004; Chen *et al.* 2018), proved capable of capturing the evolution of the microstructure. However, DEM encounters challenges in computational efficiency when dealing with irregularly shaped elements or a large number of elements. Pore-scale modelling methods for flow and mass transfer through porous media can be broadly classified into two groups: direct numerical simulation (DNS) and the pore network

model (PNM). Compared with DNS, PNM has a significant advantage in efficiency but a reduced accuracy due to simplifications of the actual structure and transport. The early PNMs used simplified regular capillary networks (Fatt 1956), which was simple but of low accuracy. This deficiency was improved significantly by extracting the network from the scanned actual structures (Lindquist *et al.* 1996; Dong & Blunt 2009). A recent progress in pore-throat segmentation (Liu *et al.* 2022) has dramatically improved the accuracy of PNM, even comparable to that of DNS. Furthermore, PNM exhibits capability in handling more intricate pore structures compared with other upscaling methods such as volume averaging and homogenization theory. The utilization of PNM has gained extensive prominence in investigating flow and transport phenomena within porous media (Bijeljic *et al.* 2004; Mehmani & Balhoff 2015; Liu & Wang 2022; Liu *et al.* 2024).

In this work, we investigate the impact of compaction on the longitudinal dispersion coefficient of porous media, utilizing a numerical framework that combines DEM and PNM. The DEM–PNM framework can effectively capture the evolution of the microstructure and efficiently simulate solute transport over a wide range of *Pe*. We reveal the non-monotonic effect of compaction on the longitudinal dispersion coefficient, which is distinguished by the presence of three distinct regimes in the variation of dispersion coefficients. The underlying mechanisms are elucidated through a comprehensive analysis of statistics of the pore structure and the flow within porous media.

2. Methods

Herein, DEM and PNM are combined to investigate the impact of compaction on the longitudinal dispersion coefficient of sphere packs. This study focuses on the scenario where the time scale of the flow is far smaller than that of the structural deformation, i.e. the flow remains in a steady state. Therefore, the structural deformation and the solute transport are decoupled. Two steps are involved in the simulation: the first step is to track the movement of each constituent particle within the sphere pack through the application of DEM simulations. This step yields the pore structure when the assembly of spheres reaches the steady state under a specific pressure load P. The second step includes the extraction of the pore network from the pore structure, followed by the implementation of PNM simulations of solute transport to obtain the dispersion coefficient D_L^P for various *Pe*. Figure 1 shows a schematic representation of the simulation procedure.

The execution of DEM simulations is accomplished utilizing the open-source software Yade (Šmilauer *et al.* 2015), within which the contact model and the integral model emerge as two crucial parts. The linear-spring-damping model (Cundall & Strack 1979) has been employed to calculate the contact forces between spheres, while the explicit integration algorithm has been utilized to update the positions of the spheres. The validity of the DEM algorithm has been substantiated through experimental data concerning the permeability–porosity relation (Tian *et al.* 2023).

The network model for flow and mass transfer has been presented in our previous work (Liu *et al.* 2024), and will not be repeated within this context. The reliability and accuracy of our PNM algorithm have been proved through rigorous validation against DNS solutions and experimental data, demonstrating relative errors of less than 5 % in predicted concentration profiles and breakthrough curves (Liu *et al.* 2024). In the simulation of flow, the pressure boundaries are implemented at both the inlet and outlet. In the context of mass transfer simulation, a constant concentration is maintained at the inlet, while a fully developed boundary condition is assumed for the outflow. The determination of the dispersion coefficient is accomplished by fitting the breakthrough curve at the outlet,
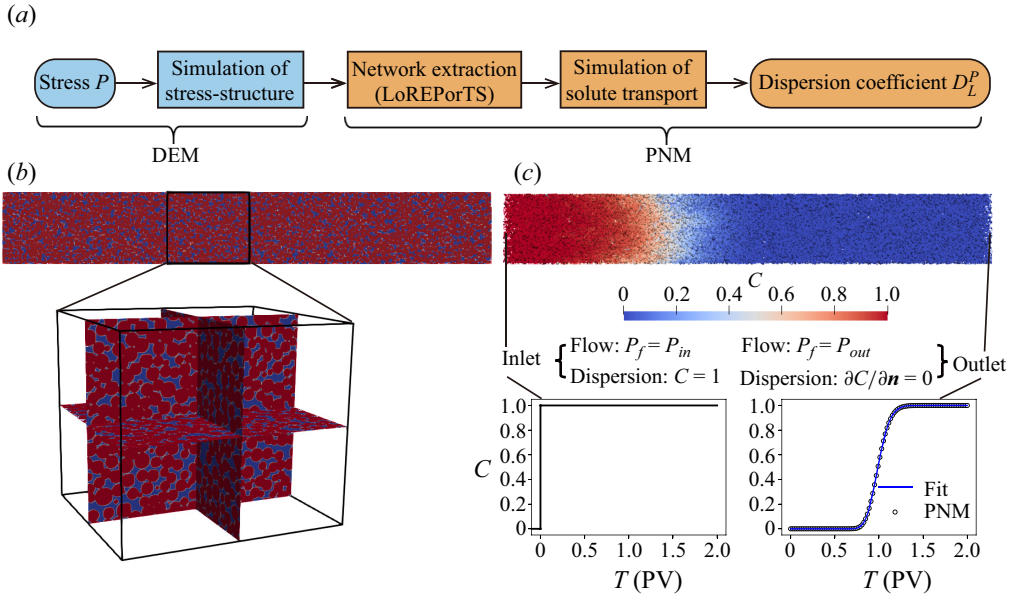
(*a*)

(*b*)

(*c*)

Figure 1. (*a*) Schematic illustration of the simulation procedure. Pore-throat segmentation is executed utilizing LoREPorTS (Liu *et al.* 2022). (*b*) Enlarged view of the pore structure for $\sigma = 0.1d_0$ and $P = 70$ MPa. (*c*) Demonstration of flow and dispersion boundary conditions and breakthrough curve fitting; P_f represents the fluid pressure and C denotes solute concentration; P_{in} and P_{out} represent the fluid pressure at the inlet and outlet, respectively; PV denotes pore volume and $\boldsymbol{n}$ is the normal vector at the outlet plane.

utilizing the analytical solution given by (Kumar, Jaiswal & Kumar 2009)

$$C(x, T) = 0.5\,\text{erfc}\left(\frac{x - UT}{2\sqrt{D_L T}}\right) + 0.5\exp\left(\frac{Ux}{D_L}\right)\text{erfc}\left(\frac{x + UT}{2\sqrt{D_L T}}\right)$$

$$- \sqrt{\frac{U^2 T}{\pi D_L}}\exp\left(\frac{UL}{D_L} - \frac{(2L - x + UT)^2}{4D_L T}\right)$$

$$+ 0.5\left(2 + \frac{U(2L - x)}{D_L} + \frac{U^2 T}{D_L}\right)\exp\left(\frac{UL}{D_L}\right)\text{erfc}\left(\frac{2L - x + UT}{2\sqrt{D_L T}}\right), \quad (2.1)$$

where D_L is the dispersion coefficient, U is the seepage velocity, T is the injection time, L is the longitudinal length of the domain, x is the observation location and C is the concentration.

3. Results and discussion

This study examines four distinct groups of sphere packs, wherein the diameters of the spheres follow a normal distribution. The grain size distributions for these four groups of sphere packs exhibit the same median $d_0 = 140\ \mu$m, but different standard deviations $\sigma = 0, 0.025d_0, 0.05d_0$ and $0.1d_0$, respectively. The pore structure of sphere packs under a specific pressure load P is obtained through DEM simulations, where P spans a range from the initial pressure load $P_0 = 5$ MPa to the maximum pressure load $P_{max} = 70$ MPa. In the simulations, the spheres are assigned a Young's modulus E of 2.5 GPa and a Poisson's ratio of 0.33. These parameters are chosen in accordance with the properties typically observed in sedimentary rocks. A total of 40 000 spheres are randomly distributed within
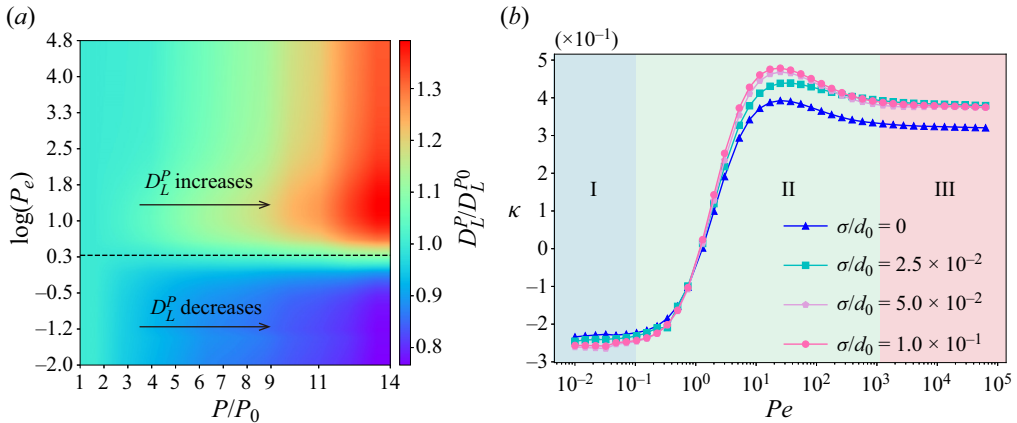
Figure 2. (a) Contour of the normalized dispersion coefficient $D_L^P/D_L^{P_0}$ of monodisperse sphere packs (i.e. $\sigma = 0$) as it varies with the normalized pressure load P/P_0 for different Pe. The dashed line represents the critical Pe_c for the shift in the trend of the dispersion coefficient with pressure load. (b) Curves of κ with Pe, where κ is the variation of dispersion coefficients.

a confined box, enclosed by rigid walls on all four sides and at the bottom. Pressure is exerted from the top, compressing the spheres on the top surface and causing them to move downward. The spheres eventually reach a stable configuration for the specific pressure load P. Interactions between spheres upon contact result in elastic deformation, altering their original spherical shape. It is important to keep in mind that the dispersion coefficient of the sphere pack may not reach an asymptotic value when the radial size or longitudinal length is small (Han, Bhakta & Carbonell 1985; Dentz, Icardi & Hidalgo 2018; Souzy *et al.* 2020). To mitigate the potential impact of domain size on the simulation outcomes, a subdomain with dimensions of $13d_0 \times 13d_0 \times 95d_0$ is cropped from the pore structure, which is utilized for the subsequent simulation of flow and mass transfer. Referring to experimental data and considering underground application scenarios (Boon *et al.* 2017), solute transport across a range of Pe spanning from 10^{-2} to $10^{4.8}$ is modelled through the manipulation of the pressure difference between the inlet and the outlet. Under laminar flow conditions, there is no limitation on the PNM simulation for the Pe range. Here Pe is defined as Ud_0/D_m, where U is the seepage velocity and the molecular diffusion coefficient D_m is 4.6×10^{-10} m^2 s^{-1}.

To present the results intuitively, the dispersion coefficient is normalized by that under the initial pressure load of $P_0 = 5$ MPa. Figure 2(a) illustrates the normalized dispersion coefficient $(D_L^P/D_L^{P_0})$ as it varies with the pressure load for different Pe, from which a non-monotonic dependence is observed. Specifically, at small Pe, the dispersion coefficient exhibits a negative dependence on the pressure load; however, the dependence shifts to a positive type as Pe increases, which is consistent with experimental observations (Charlaix *et al.* 1987; Huh *et al.* 1988; Östergren & Trägårdh 2000; Hamamoto *et al.* 2009; Kuncoro *et al.* 2014). We define the variation in dispersion coefficients as $\kappa = (D_L^{P_{max}}/D_L^{P_0}) - 1$, where $D_L^{P_0}$ and $D_L^{P_{max}}$ are the dispersion coefficients corresponding to the initial pressure load $P_0 = 5$ MPa and the maximum pressure load $P_{max} = 70$ MPa, respectively. The sign and absolute value of κ reveal the trend and sensitivity of the dispersion coefficient with pressure load, respectively. Notably, the variation of κ with Pe manifests three distinct regimes (figure 2b). Regime I ($Pe < 0.1$): κ demonstrates a negative value while maintaining a consistent Pe-independence. Regime II ($0.1 < Pe <$

1000): κ exhibits a transition from a negative to a positive value, reaching its peak at approximately $Pe = 30$, and subsequently declining to a positive plateau. Regime III ($Pe > 1000$): κ remains positive and invariant with Pe. The four groups of sphere packs exhibit a similar relationship between the dispersion coefficient and the pressure load. For conciseness, we only elaborate on the results and analyses for monodisperse sphere packs (i.e. $\sigma = 0$), while those associated with polydisperse sphere packs (i.e. $\sigma = 0.025d_0, 0.05d_0$ and $0.1d_0$) will be briefly presented at the end of this section. Throughout the subsequent discussion, it is important to note that the sphere packs refer to the monodisperse sphere packs unless otherwise stated.

What are the underlying mechanisms responsible for the diverse regimes of κ as it varies with Pe? Under laminar flow conditions, the physical mechanisms contributing to dispersion encompass molecular diffusion, shear dispersion, hold-up dispersion and mechanical dispersion (Koch & Brady 1985). Molecular diffusion is the random thermal motion of solute molecules or particles. Shear dispersion, also known as boundary-layer dispersion, is caused by non-uniform velocity profiles within pores or throats. According to classical theories of dispersion (Koch & Brady 1985; Sahimi *et al.* 1986), hold-up dispersion arises from the retention effect of solute species in zero-velocity regions where species can escape only by molecular diffusion, such as the interior of permeable solid grains or dead-ends. Nevertheless, this study demonstrates that low-velocity regions in porous media flow, where flow does exist but is weak, are equally capable of producing hold-up dispersion. Mechanical dispersion is the result of repeated separation and merging of flow passages at the junctions of the pore space. At small Pe, the impact of convection is negligible, and the predominant mechanism is molecular diffusion. As Pe increases, convection exerts an increasingly important influence on dispersion. When Pe reaches a significant magnitude, the dominant mechanism switches to mechanical dispersion, while in the intermediate range of Pe, the aforementioned four mechanisms operate collectively.

To assess the impact of heightened compaction on dispersion mechanisms, the first task is to explore the changes in the pore structure, along with the subsequent modifications in the flow within the porous medium. As the pressure load increases from the initial pressure load $P_0 = 5$ MPa to the maximum pressure load $P_{max} = 70$ MPa, the pore structure of sphere packs becomes significantly tighter. As depicted in figure 3(*a*), the porosity ϕ exhibits a decline from 0.362 to 0.247, along with a decrease in permeability K from 12.6 mD to 3.8 mD. The coefficient of variation of pore radii, defined as $CV_R = std(R)/\langle R \rangle$, where $std(R)$ and $\langle R \rangle$ denote the standard deviation and mean of the pore radii, respectively, exhibits an increasing trend as the pressure load increases (figure 3*b*). This trend signifies the intensified heterogeneity of the pore structure. The disorder of the porous media flow is characterized by the coefficient of variation of throat flow rates, defined as $CV_{q_{ij}} = std(q_{ij})/\langle q_{ij} \rangle$, where $std(q_{ij})$ and $\langle q_{ij} \rangle$ denote the standard deviation and mean of throat flow rates, respectively. The number and volume ratio of dead-end pores always remain less than three-thousandths and one-thousandth, respectively, implying the negligible role of dead-ends. This aligns with literature (Koch & Brady 1985), asserting the absence of zero-velocity regions within sphere packs. Despite the rarity of dead-ends within the sphere packs, a substantial presence of low-velocity zones is evident (figure 4*a,c*), characterized by weak flow and termed as stagnant zones. The stagnant zones are determined based on the transit times within pores and throats, the procedures of which are described in detail in the Appendix. The volume and number fractions of the stagnant zone increase significantly with pressure loads and can be as high as 0.35 (figure 4*c*). Previous literature has acknowledged the existence of these low-velocity regions in porous media flow, with predictions that these regions may exert an influence on dispersion (Reynolds & Harral 2000). We further demonstrate that these stagnant
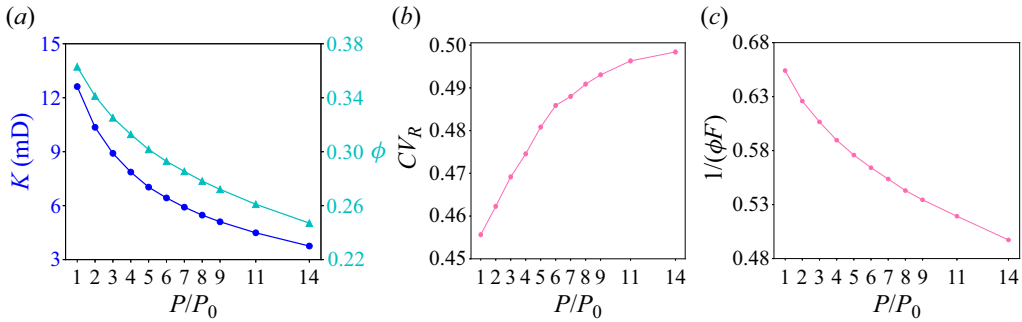
Figure 3. Evolution of pore structure characteristics with the normalized pressure load P/P_0: (*a*) porosity ϕ and permeability K; (*b*) coefficient of variation of pore radii, CV_R; (*c*) values of $1/(\phi F)$, where ϕ and F represent porosity and formation factor, respectively.
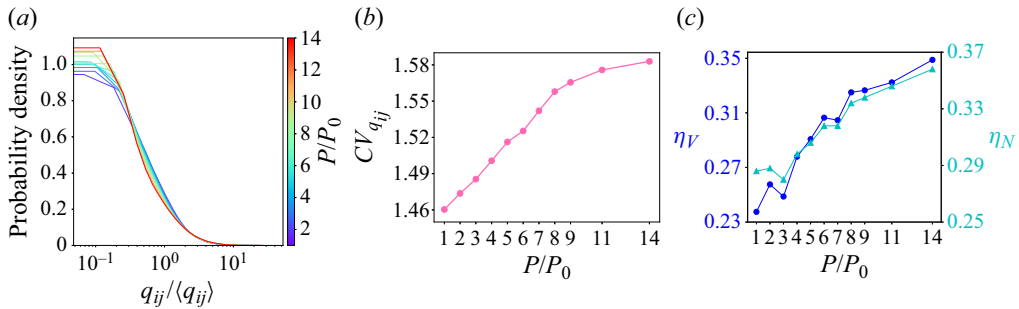

Figure 4. Evolution of flow field characteristics with the normalized pressure load P/P_0: (*a*) probability density distribution of the normalized throat flow rate $q_{ij}/\langle q_{ij} \rangle$; (*b*) coefficient of variation of throat flow rate, $CV_{q_{ij}}$; (*c*) volume fraction η_V and number fraction η_N of the low-velocity zone to the whole pore space.

zones resemble dead-ends in inducing a retention effect on solute species, consequently resulting in hold-up dispersion. Notably, flow does occur within the stagnant zone, albeit at a significantly lower rate compared with the average flow through the porous medium. In the intermediate *Pe* range, advection governs tracer transport outside stagnant zones, while molecular diffusion dominates tracer transport inside stagnant zones. In this scenario, similar to zero-velocity regions (Koch & Brady 1985), the stagnant zone induces hold-up dispersion. As *Pe* increases, solute transport within the stagnant zone shifts towards dominance by advection, resulting in the disappearance of the hold-up effect. Hence, the stagnant zone exclusively generates hold-up dispersion within the intermediate *Pe* range. However, it is crucial to acknowledge that stagnant zones and zero-velocity regions do exhibit distinct characteristics. Conversely, regardless of *Pe*, solute transport through zero-velocity regions remains consistently governed by molecular diffusion. Consequently, zero-velocity regions generate hold-up dispersion without an upper limit on *Pe*. For the domain size considered here, if advection weakens or disappears within the stagnant zone, dispersion transitions from Fickian to non-Fickian at large *Pe*, further emphasizing this distinction.

In regime I, molecular diffusion emerges as the dominant mechanism governing dispersion, wherein the dispersion coefficient D_L^P relies solely on the nature of the pore structure, rendering it independent of *Pe*. The dispersion coefficient D_L^P can be expressed as $D_L^P/D_m = 1/(\phi F)$, where F is the formation factor and ϕ is the porosity. The formation

988 R2-7

factor defines the normalized electrical resistance of the pore structure, analogous to the absolute permeability of porous media. A detailed description of how PNM calculates the formation coefficient has been provided in our previous work (Liu *et al.* 2024). The magnitude of $1/(\phi F)$ experiences a reduction with the increase of pressure load (figure 3*c*), which explains the negative value of κ.

In regime III, mechanical dispersion dominates, exhibiting a linear relationship between the dispersion coefficient D_L^P and the Péclet number *Pe*, denoted as $D_L^P = \alpha^P Pe$ (Sahimi *et al.* 1986; Bruderer & Bernabé 2001; Bijeljic *et al.* 2004). Some studies also suggested that D_L^P may exhibit a logarithmic scaling at large *Pe*, such as $D_L^P \sim Pe \log(Pe)$ (Saffman 1959; Koch & Brady 1985; Puyguiraud *et al.* 2021), a phenomenon which was not observed in this study. Here α^P represents the dispersivity of the sphere pack, a quantity that depends on the nature of porous media flow. Specifically, the stronger the disorder of the flow, the larger the value of α^P is. We have $\kappa = (\alpha^{P_{max}}/\alpha^{P_0}) - 1$, where α^{P_0} and $\alpha^{P_{max}}$ denote the dispersivity of the sphere pack at the initial pressure load P_0 and the maximum pressure load P_{max}, respectively. The influence of *Pe* is cancelled out by the ratio of $D_L^{P_{max}}$ and $D_L^{P_0}$, implying that κ is independent of *Pe*. Furthermore, the heterogeneity of the pore structure CV_R is enhanced with increasing pressure load (figure 3*b*), which strengthens the disorder $CV_{q_{ij}}$ of the flow (figure 4*b*), consequently accentuating the strength of mechanical dispersion (Sahimi *et al.* 1986; Bruderer & Bernabé 2001). This ultimately leads to an increase in the dispersivity, i.e. $\alpha^{P_{max}} > \alpha^{P_0}$. Therefore, κ maintains a positive plateau in this regime.

In regime II, both advection and diffusion play significant roles. This regime is characterized by the competition of multiple dispersion mechanisms, encompassing molecular diffusion, shear dispersion, hold-up dispersion, and mechanical dispersion. From the analyses on regimes I and III, it is demonstrated that molecular diffusion is weakened while mechanical dispersion is enhanced with increasing pressure load. Still, we need to figure out the impact of heightened compaction on shear dispersion and hold-up dispersion.

We examine the significance of shear dispersion through comparisons of dispersion coefficients that incorporate or exclude the effect of shear dispersion. The effect of shear dispersion is incorporated by utilizing shear dispersion coefficients in the calculation of diffusive mass transfer fluxes in the network model. These shear dispersion coefficients encapsulate the influence of parabolic velocity profiles on longitudinal mass transfer within a single pore or throat. Conversely, replacing the shear dispersion coefficient with the molecular diffusion coefficient implies disregarding the influence of parabolic velocity profiles, thereby deactivating the shear dispersion effect (Liu *et al.* 2024). This action does not alter stochastic fluctuations or the low-velocity regions within the porous media flow. Consequently, mechanical dispersion and stagnant dispersion remain unaffected. Figure 5(*a*) illustrates that the influence of shear dispersion on the dispersion coefficient is of minimal consequence, constituting less than 6 %. This observation aligns consistently with our earlier findings that when the pore structure is highly disordered, the contribution of shear dispersion to the overall picture will be small (Liu *et al.* 2024).

According to classical theories of dispersion (Koch & Brady 1985; Sahimi *et al.* 1986), the essence of hold-up dispersion lies in the retention effect of solutes in dead-ends and the interior of permeable grains. Negligible dead-ends exist within the sphere packs, and given the consideration of impermeable grains in this study, one might question the presence of hold-up dispersion within the sphere packs. Nevertheless, our analysis confirms the presence of hold-up dispersion. If hold-up dispersion is absent, and considering the negligible role of shear dispersion, the dispersion within regime II transitions from
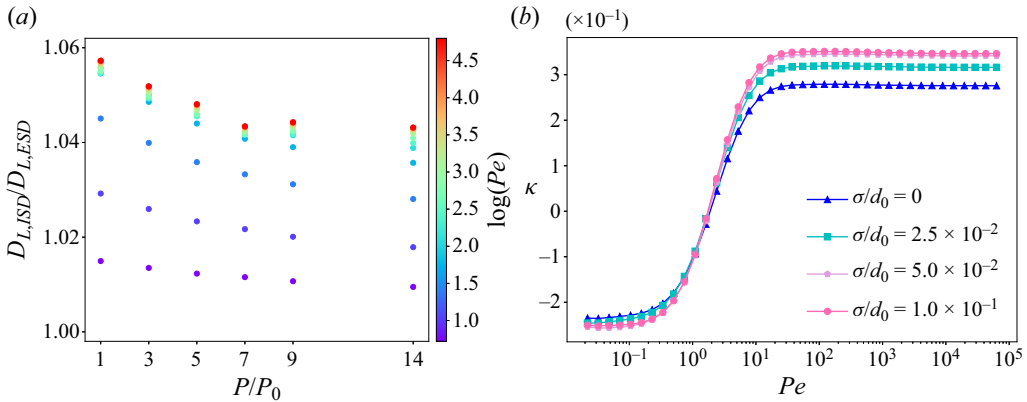
Figure 5. (*a*) Impact of shear dispersion on the dispersion coefficient; $D_{L,ISD}$ and $D_{L,ESD}$ are the dispersion coefficients that incorporate and exclude the effect of shear dispersion, respectively. (*b*) Variation of κ with Pe when the effect hold-up dispersion is excluded by setting the volume of the low-velocity region to zero, where κ is the variation of dispersion coefficients.

weakened molecular diffusion dominance to enhanced mechanical dispersion dominance with increasing Pe. As the effects of molecular diffusion and mechanical dispersion on κ are independent of Pe, κ is expected to exhibit a smooth transition from negative to positive values with increasing Pe. Nevertheless, this expectation contradicts the peak observed in the κ–Pe curve. This discrepancy implies the presence of an additional mechanism, in conjunction with mechanical dispersion, which is enhanced with increasing pressure load and acts only near the peak. We speculate that this additional mechanism is hold-up dispersion, generated by the large number of stagnant regions where there is flow but weak. The significant increase in both the number and volume fraction of stagnant regions with rising pressure load implies an enhancement of the hold-up dispersion they generate, aligning with the observed peak in the κ–Pe curve. We eliminate the hold-up dispersion by assigning zero volumes to pores and throats within stagnant zones while keeping other parameters constant as in the base case where hold-up dispersion is incorporated. Hold-up dispersion is attributed to the hysteresis between the concentration within the stagnant zone and the neighbouring active zone. Therefore, by setting the volume of the pores and throats within stagnant zones to zero, the stagnant zone will consistently maintain the same concentration as the adjacent active zone, i.e. the hold-up effect is turned off. The exclusion of hold-up dispersion leads to the disappearance of the peak in the κ–Pe curve (figure 5*b*), providing additional confirmation of our conjecture. To our best knowledge, this discovery is reported for the first time in this study.

To conclude, the mechanisms that essentially play roles in regime II involve molecular diffusion, hold-up dispersion and mechanical dispersion. With increasing pressure load, the weakening of molecular diffusion competes with the enhancement of hold-up dispersion and mechanical dispersion, collectively determining the dispersion coefficient in this regime. On the other hand, as Pe increases, convection exerts an increasingly important influence on dispersion, leading to an evolution of dispersion from one initially dominated by molecular diffusion to one that is jointly dominated by hold-up dispersion and mechanical dispersion. The shift in the dominance of dispersion mechanisms leads to a change in κ from a negative to a positive value, i.e. the dependence between the dispersion coefficient and the pressure load changes from negative to positive. The value of κ reaches its peak at approximately $Pe = 30$ and subsequently undergoes a decline. This trend is
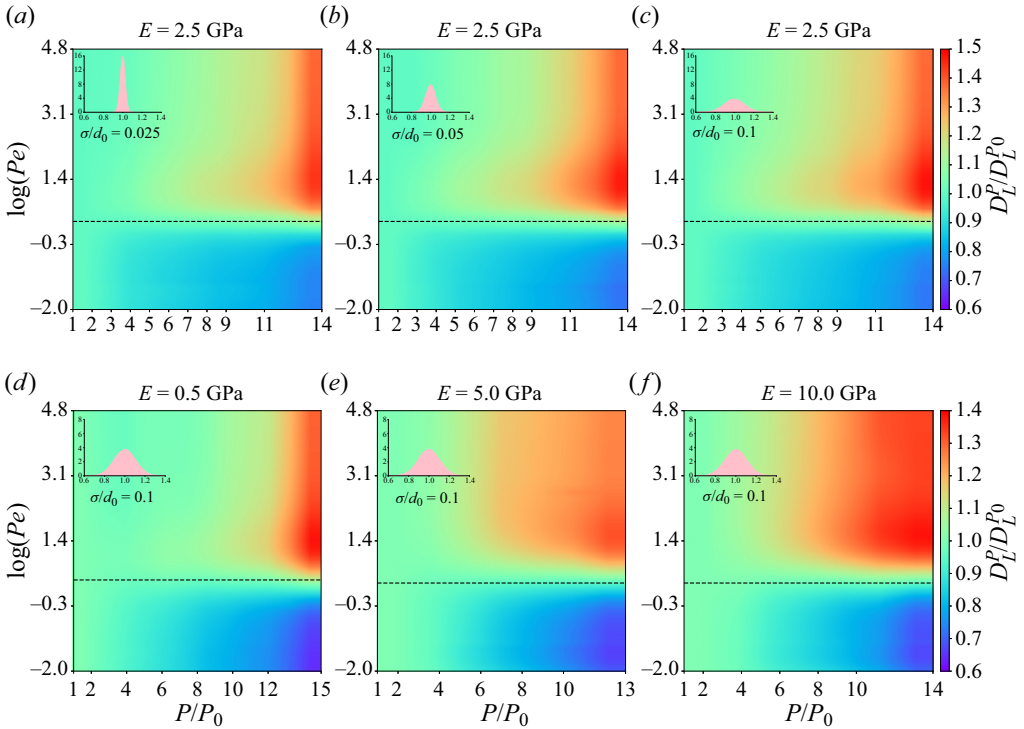
Figure 6. The normalized dispersion coefficient $D_L^P/D_L^{P_0}$ of polydisperse sphere packs as it varies with the normalized pressure load P/P_0 for different Pe. The Young's modulus E of the spheres in (a–c) is 2.5 GPa, while E in (d–f) is 0.5 GPa, 5.0 GPa, 10 GPa, respectively. The initial pressure load P_0 in (a–c) is 5 MPa, while P_0 in (d–f) is 1 MPa, 10 MPa, 20 MPa, respectively. Insets illustrate the probability density distribution of sphere diameter d of the corresponding sphere packs, where the horizontal axis represents the normalized diameter d/d_0, while the vertical axis represents the probability density. The standard deviations σ of the sphere diameters are as follows: (a) $\sigma = 0.025d_0$, (b) $\sigma = 0.05d_0$, (c) $\sigma = 0.1d_0$, (d) $\sigma = 0.1d_0$, (e) $\sigma = 0.1d_0$, (f) $\sigma = 0.1d_0$.

explained by the conjecture that hold-up dispersion diminishes as Pe exceeds 30, leading to a shift in the increase of the dispersion coefficient from being driven by a combination of hold-up dispersion and mechanical dispersion to being driven by mechanical dispersion only.

Figure 6(a–c) shows the normalized dispersion coefficient $D_L^P/D_L^{P_0}$ of the three groups of polydisperse sphere packs (i.e. $\sigma = 0.025d_0$, $0.05d_0$ and $0.1d_0$) as it varies with the pressure load across various Pe, which is exactly the same as in the case of monodisperse sphere packs (i.e. $\sigma = 0$). Furthermore, with increasing pressure load, the evolution of statistics of the pore structure and the flow field of both monodisperse and polydisperse sphere packs are consistent. Hence, the conclusions drawn from the analysis based on monodisperse sphere packs are equally applicable to the case of polydisperse sphere packs. Moreover, it is noted that these analyses and conclusions also hold true for sphere packs with different Young's modulus (figure 6d–f), further validating the generality of this study. Due to space limitations, a detailed elaboration on the structure and flow analyses of polydisperse sphere packs is omitted here. In this study, the standard deviation σ of the sphere diameter is limited to a maximum of $0.1d_0$ due to the constraints of computational

988 R2-10

cost associated with DEM. We believe that the conclusions of this study are equally applicable to sphere packs with a broader grain size distribution.

4. Conclusions

We study the impact of compaction on longitudinal dispersion coefficient of porous materials through a DEM-PNM numerical framework. We reveal the non-monotonic effect of compaction on dispersion coefficient, which is distinguished by the presence of three distinct regimes in the variation of dispersion coefficients (κ) across various *Pe*. The analysis of the statistics of the pore structure and the flow field elucidates the origin of the phenomenon: compaction exerts disparate impacts on the mechanisms of dispersion. Specifically, the porous medium tightens with increasing pressure load, reducing the effect of molecular diffusion that primarily governs at small *Pe*. On the other hand, the elevated pressure load enhances the heterogeneity of the pore structure, leading to enhanced disorder and an elevated proportion of stagnant regions within the porous media flow. These enhancements further strengthen mechanical dispersion and hold-up dispersion, respectively, both acting at larger *Pe*. It is essential to emphasize that hold-up dispersion arises from stagnant regions characterized by weak flow, which differ fundamentally from zero-velocity regions (dead-ends or the interior of permeable grains) as described in classical theories of dispersion (Koch & Brady 1985; Sahimi *et al.* 1986). The competition between the weakening of molecular diffusion and the enhancement of hold-up dispersion and mechanical dispersion, together with the shift in the dominance of dispersion mechanisms across various *Pe*, results in the multiple regimes in the κ–*Pe* curve. Our study sheds light on the guidance for structural design and modulation of the dispersion coefficient of packed porous materials.

Declaration of interests. The authors report no conflict of interest.

Author ORCIDs.

 Moran Wang https://orcid.org/0000-0002-0112-5150.

Author contributions. M.W. conceived and promoted this work. Y.L. performed the simulations and analysis. Y.L. wrote the paper and M.W. revised the text. W.G. and H.X. performed the simulations and revised the text.

Appendix

Identification of stagnant zones involves the following steps: first, transit times V/q through network elements (pores and throats) are sorted in descending order, with V and q denoting the volume and flow rate of network elements, respectively. The sorted network elements are labelled from 1 to N_0 according to their sorting index, where N_0 denotes the total number of network elements. Following this, network elements are removed from the network, giving priority to those with smaller labels. The number of network elements removed is quantified by the removal ratio N/N_0, indicating the removal of all network elements with labels less than N. Subsequently, the permeability K of the pore network for the removal ratio N/N_0 is determined, showing a decrease with N/N_0. Next, the derivative $\delta(K/K_0)/\delta(N/N_0)$ of the normalized permeability K/K_0 to the removal ratio N/N_0 is calculated, where K_0 denotes the permeability of the original network. The removal ratio corresponding to when $\delta(K/K_0)/\delta(N/N_0) = -1$ is denoted as N_c/N_0. The stagnant zone consists of the sorted network elements with labels $N < N_c$. We emphasize

that the exclusion of hold-up dispersion is achieved by assigning zero volumes to the stagnant zones, rather than by removing stagnant zones from the network.

References

AMOOIE, M.A., SOLTANIAN, M.R. & MOORTGAT, J. 2018 Solutal convection in porous media: comparison between boundary conditions of constant concentration and constant flux. *Phys. Rev.* E **98** (3), 033118.

BIJELJIC, B., MOSTAGHIMI, P. & BLUNT, M.J. 2011 Signature of non-Fickian solute transport in complex heterogeneous porous media. *Phys. Rev. Lett.* **107** (20), 204502.

BIJELJIC, B., MUGGERIDGE, A.H. & BLUNT, M.J. 2004 Pore-scale modeling of longitudinal dispersion. *Water Resour. Res.* **40** (11), W11501.

BOLSTER, D. 2014 The fluid mechanics of dissolution trapping in geologic storage of CO2. *J. Fluid Mech.* **740**, 1–4.

BOON, M., BIJELJIC, B. & KREVOR, S. 2017 Observations of the impact of rock heterogeneity on solute spreading and mixing. *Water Resour. Res.* **53** (6), 4624–4642.

BORDOLOI, A.D., SCHEIDWEILER, D., DENTZ, M., BOUABDELLAOUI, M., ABBARCHI, M. & DE ANNA, P. 2022 Structure induced laminar vortices control anomalous dispersion in porous media. *Nat. Commun.* **13** (1), 3820.

BORGNE, T.L., DENTZ, M., BOLSTER, D., CARRERA, J., DE DREUZY, J.-R. & DAVY, P. 2010 Non-fickian mixing: temporal evolution of the scalar dissipation rate in heterogeneous porous media. *Adv. Water Resour.* **33** (12), 1468–1475.

BRUDERER, C. & BERNABÉ, Y. 2001 Network modeling of dispersion: transition from taylor dispersion in homogeneous networks to mechanical dispersion in very heterogeneous ones. *Water Resour. Res.* **37** (4), 897–908.

CHARLAIX, E., HULIN, J.P. & PLONA, T.J. 1987 Experimental study of tracer dispersion in sintered glass porous materials of variable compaction. *Phys. Fluids* **30** (6), 1690–1698.

CHEN, Z., JIN, X. & WANG, M. 2018 A new thermo-mechanical coupled dem model with non-spherical grains for thermally induced damage of rocks. *J. Mech. Phys. Solids* **116**, 54–69.

CUNDALL, P.A. & STRACK, O.D. 1979 A discrete numerical model for granular assemblies. *Geotechnique* **29** (1), 47–65.

DENTZ, M., CREPPY, A., DOUARCHE, C., CLÉMENT, E. & AURADOU, H. 2022 Dispersion of motile bacteria in a porous medium. *J. Fluid Mech.* **946**, A33.

DENTZ, M., HIDALGO, J.J. & LESTER, D. 2023 Mixing in porous media: concepts and approaches across scales. *Transp. Porous Media* **146** (1-2), 5–53.

DENTZ, M., ICARDI, M. & HIDALGO, J.J. 2018 Mechanisms of dispersion in a porous medium. *J. Fluid Mech.* **841**, 851–882.

DONG, H. & BLUNT, M.J. 2009 Pore-network extraction from micro-computerized-tomography images. *Phys. Rev.* E **80** (3), 036307.

FATT, I. 1956 The network model of porous media. *Trans. AIME* **207** (01), 144–181.

GOLDOBIN, D.S. 2011 Scaling of transport coefficients of porous media under compaction. *Europhys. Lett.* **95** (6), 64004.

HAMAMOTO, S., PERERA, M.S.A., RESURRECCION, A., KAWAMOTO, K., HASEGAWA, S., KOMATSU, T. & MOLDRUP, P. 2009 The solute diffusion coefficient in variably compacted, unsaturated volcanic ash soils. *Vadose Zone J.* **8** (4), 942–952.

HAN, N.W., BHAKTA, J. & CARBONELL, R.G. 1985 Longitudinal and lateral dispersion in packed beds: effect of column length and particle size distribution. *AlChE J.* **31** (2), 277–288.

HUH, J.P., CHARLAIX, E. & PLONA, T.J. 1988 Tracer dispersion in sintered glass beads with a bidisperse size distribution. *AlChE J.* **34** (4), 610–617.

JURTZ, N., KRAUME, M. & WEHINGER, G.D. 2019 Advances in fixed-bed reactor modeling using particle-resolved computational fluid dynamics (CFD). *Rev. Chem. Engng* **35** (2), 139–190.

KANG, P.K., LEI, Q., DENTZ, M. & JUANES, R. 2019 Stress-induced anomalous transport in natural fracture networks. *Water Resour. Res.* **55** (5), 4163–4185.

KOCH, D.L. & BRADY, J.F. 1985 Dispersion in fixed beds. *J. Fluid Mech.* **154**, 399–427.

KUMAR, A., JAISWAL, D.K. & KUMAR, N. 2009 Analytical solutions of one-dimensional advection-diffusion equation with variable coefficients in a finite domain. *J. Earth Syst. Sci.* **118**, 539–549.

KUNCORO, P.H., KOGA, K., SATTA, N. & MUTO, Y. 2014 A study on the effect of compaction on transport properties of soil gas and water I: relative gas diffusivity, air permeability, and saturated hydraulic conductivity. *Soil Tillage Res.* **143**, 172–179.

LINDQUIST, W.B., LEE, S.M., COKER, D.A., JONES, K.W. & SPANNE, P. 1996 Medial axis analysis of void structure in three-dimensional tomographic images of porous media. *J. Geophys. Res.: Solid Earth* **101** (B4), 8297–8310.

LIU, Y., GONG, W., XIAO, H. & WANG, M. 2024 A pore-scale numerical framework for solute transport and dispersion in porous media. *Adv. Water Resour.* **183**, 104602.

LIU, Y., GONG, W., ZHAO, Y., JIN, X. & WANG, M. 2022 A pore-throat segmentation method based on local hydraulic resistance equivalence for pore-network modeling. *Water Resour. Res.* **58** (12), e2022WR033142.

LIU, F. & WANG, M. 2022 Trapping patterns during capillary displacements in disordered media. *J. Fluid Mech.* **933**, A52.

MEHMANI, Y. & BALHOFF, M.T. 2015 Eulerian network modeling of longitudinal dispersion. *Water Resour. Res.* **51** (10), 8586–8606.

MORRIS, J.P., HAO, Y., FOXALL, W. & MCNAB, W. 2011 A study of injection-induced mechanical deformation at the in salah CO2 storage project. *Intl J. Greenh. Gas Control* **5** (2), 270–280.

ÖSTERGREN, K.C.E. & TRÄGÅRDH, C. 2000 Characterization of hydrodynamic dispersion in a chromatographic column under compression. *Chem. Engng J.* **79** (2), 103–111.

PETERS, G.P. & SMITH, D.W. 2002 Solute transport through a deforming porous medium. *Intl J. Numer. Anal. Meth. Geomech.* **26** (7), 683–717.

POTYONDY, D.O. & CUNDALL, P. 2004 A bonded-particle model for rock. *Intl J. Rock Mech. Min. Sci.* **41** (8), 1329–1364.

PUYGUIRAUD, A., GOUZE, P. & DENTZ, M. 2021 Pore-scale mixing and the evolution of hydrodynamic dispersion in porous media. *Phys. Rev. Lett.* **126** (16), 164501.

QIU, J., CHEN, X. & TONG, J. 2022 Fully transient analytical solution for solute transport in 1D deforming saturated porous media considering nonlinear compressibility and permeability. *Appl. Math. Model.* **108**, 122–141.

RANJITH, P. & PERERA, M. 2011 A new triaxial apparatus to study the mechanical and fluid flow aspects of carbon dioxide sequestration in geological formations. *Fuel* **90** (8), 2751–2759.

REYNOLDS, S.V.R.A.M. & HARRAL, B.B. 2000 Flow and dispersion through a close-packed fixed bed of spheres. *Phys. Rev.* E **62** (3), 3632.

RINGROSE, P., MATHIESON, A., WRIGHT, I., SELAMA, F., HANSEN, O., BISSELL, R., SAOULA, N. & MIDGLEY, J. 2013 The in salah CO2 storage project: lessons learned and knowledge transfer. *Energy Procedia* **37**, 6226–6236.

SAFFMAN, P.G. 1959 A theory of dispersion in a porous medium. *J. Fluid Mech.* **6** (3), 321–349.

SAHIMI, M., HUGHES, B.D., SCRIVEN, L.E. & DAVIS, H.T. 1986 Dispersion in flow through porous media–I. One-phase flow. *Chem. Engng Sci.* **41** (8), 2103–2122.

ŠMILAUER, V., CATALANO, E., CHAREYRE, B., DOROFEENKO, S., DURIEZ, J., DYCK, N., ELIAS, J., ER, B., EULITZ, A. & GLADKY, A. 2015 Yade documentation 2nd ed. The yade project. *Transp. Porous Media*.

SMITH, D.W. 2000 One-dimensional contaminant transport through a deforming porous medium: theory and a solution for a quasi-steady-state problem. *Intl J. Numer. Anal. Meth. Geomech.* **24** (8), 693–722.

SOUZY, M., LHUISSIER, H., MÉHEUST, Y., LE BORGNE, T. & METZGER, B. 2020 Velocity distributions, dispersion and stretching in three-dimensional porous media. *J. Fluid Mech.* **891**, A16.

TIAN, Z., ZHANG, D., ZHOU, G., ZHANG, S. & WANG, M. 2023 Compaction and sintering effects on scaling law of permeability-porosity relation of powder materials. *Intl J. Mech. Sci.* **256**, 108511.